Insurance Institute for Business & Home Safety®

Wind Loads on Discontinuous Metal Roofing

Dr. Murray J. Morrison

Connell Miller

July 2017

Introduction

Wind loads on air-permeable, multi-layer roofing systems such as discontinuous metal roofing (DMR) are complicated because the details affecting how the pressures are transmitted to each layer are poorly understood. Pressure equalization, the mechanism whereby pressures on external building surfaces are partially transmitted through air-permeable outer layers to interior layers, is known to occur, but is not currently well defined. Little design guidance is available in building codes, which contain no specific provisions for estimating loads on air-permeable, multi-layer systems.

Pressure equalization generally follows the same basic rules and physics associated with internal pressures in buildings. When wind-induced external pressures are applied to a building with openings in the building envelope, such as the ones created at the joints connecting the pieces of DMR, the external pressures are transmitted through the openings to the cavity between the cladding and the sheathing of the building. Pressure equalization of roof cladding systems depends on the gaps between panels, the volume and shape of the cavity between layers, the size of the panels, and the external pressures on the roof. The flexibility of the cladding will also play a minor role. As gaps between panels, which provide the route for air flow into or out of the cavity, become smaller, the level of pressure equalization decreases, increasing the net wind loads on the cladding layer. Large external pressure gradients and larger cavity volumes tend to increase the net wind loads as well (Oh and Kopp, 2014).

The net wind loads on cladding are usually defined using a pressure equalization factor (PEF),

$$PEF(x) = \frac{P_{external} - P_{deck}}{P_{external}} = \frac{P_{net}}{P_{external}} \quad [1]$$

where $P_{external}$ represents the external pressure on the cladding, P_{deck} represents the pressure between the roof deck and the underside of the cladding and P_{net} represents the net pressure between the top and bottom surfaces. Thus, the PEF represents the proportion of load acting on the cladding layer.

Understanding pressure equalization is crucial to understanding how loading is transferred through multi-layer systems and, ultimately, to understanding the wind load that each portion of the roof or wall assembly must resist. Certain product test standards, such as the one for PVC siding, ASTM D3679-13 (2013), take advantage of pressure equalization by reducing the required test pressure that the product must resist to meet the required design pressure. Morrison and Cope (2015) conducted a study of multi-layer wall systems using several different types of exterior sidings and found that the average PEF varies from 0.4 to 0.8, depending on the product. Miller et al. (2017), utilizing the full-scale measurements from Morrison and Cope (2015), have shown that it is possible to determine PEF values for products by using a multiple airbox technique.

The current work applies the methodology of Morrison and Cope (2015) to determine the PEF values for two DMR systems in the Insurance Institute for Business & Home Safety (IBHS) full-scale wind tunnel. The results of this study are summarized herein.

Experimental Setup

The experiments were carried out in IBHS' large test chamber. The test chamber is capable of testing one- and two-story, full-scale buildings to realistic boundary layer winds. The current experiments were conducted using a flow field of a typical open-country terrain with a roughness length, z_o, of 0.01 m. Complete details of the IBHS test chamber and flow field characteristics can be found in Standohar-Alfano et al. (2017).

Specimen

A typical single-story residential structure with plan dimensions of 30 ft x 40 ft was used in this study. The mean roof height of the building was 17 ft and had a slope of 4:12. The roof was a hip-gable construction; one end of the building had a gable end and the other had a hip end. The roof of the building was built following typical construction practices with oriented strand board (OSB) sheathing and a 30-lb felt with 6-inch lap underlayment. Two different types of DMR were installed, each taking up one half of the roof. The products selected for testing were determined by the Metal Construction Association and provided to IBHS. Both products were jointly installed by IBHS staff and product manufacturer representatives to ensure the products were installed in accordance with manufacturer guidelines. Figure 1 shows the installation of both products on the roof of the building. Figure 1 (Top) shows the installation of Gerard Canyon Shake metal roof panels (referred to as DMR1 for the remainder of this report) on battens attached to the roof sheathing. Figure 1 (Bottom) shows the installation of Advanta metal shingles (referred to as DMR2 for the remainder of this report), which are attached directly to the roof sheathing. Figure 2 shows a photograph of the completed test building located on the turntable inside the IBHS test chamber.

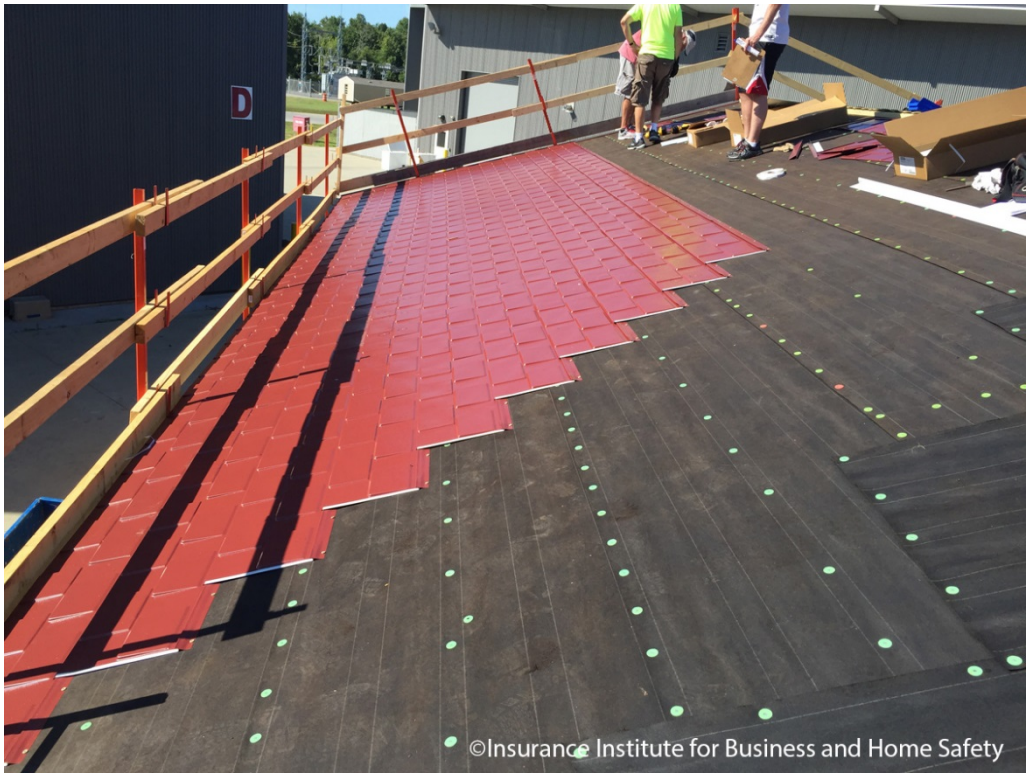

***Figure 1**. Installation of the two DMR products tested at IBHS. Top: Gerard Canyon Shake metal roof panels (DMR1); Bottom: Advanta metal shingles (DMR2).*

Figure 2. *Completed test building located in the IBHS test chamber.*

Instrumentation

During the installation of both products, pressure taps to measure the wind pressures were installed on select panels throughout the entire roof. The pressures were measured at either one or six locations on a single panel depending on its location on the roof. Figure 3 shows the layout of instrumented panels and measurement locations for both DMR1 and DMR2. Differences in the airspace between the roof cover and roof deck of each product result in different layouts for each product.

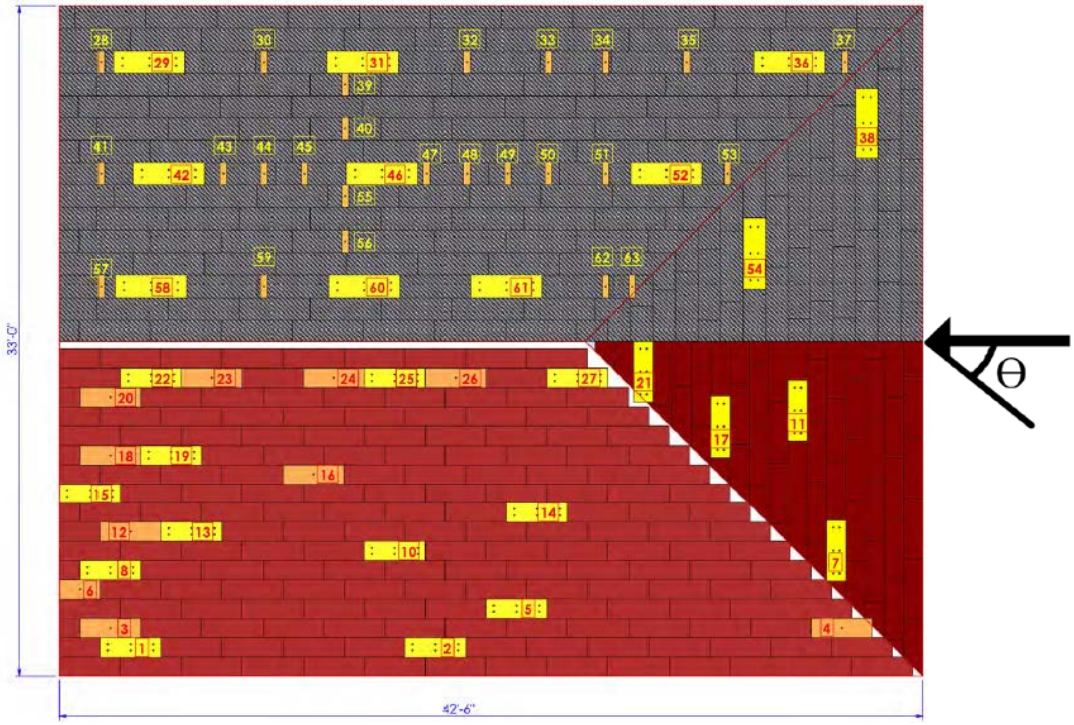

Figure 3. *Panel locations with panel numbers. Yellow indicates an instrumented panel with black dots indicating location of each pressure tap. Top (gray)–DMR1; Bottom (red)–DMR2.*

Table 3 in Appendix A provides the panel numbers and number of pressure tap locations for each product. At each location where the pressure was measured, two pressure taps were installed to allow the measurement of pressures on the outside (external) surface and the measurement of net pressure between the external and cavity pressures. The first pressure tap is mounted with its opening flush with the outside surface of the metal roofing. The second pressure tap is mounted with its opening flush with the roof sheathing. Two differential pressure transducers are used to directly measure the external pressure and the net pressure across the metal roofing. Figure 4 provides a schematic of the pressure tap locations and the pressure transducer configuration at each tap location to measure both net and external pressures. Figure 5 shows the transducers installed underneath the roof sheathing. In total, pressures are measured at 91 and 106 locations for DMR1 and DMR2, respectively, resulting in a total of 394 pressure transducers over the entire roof.

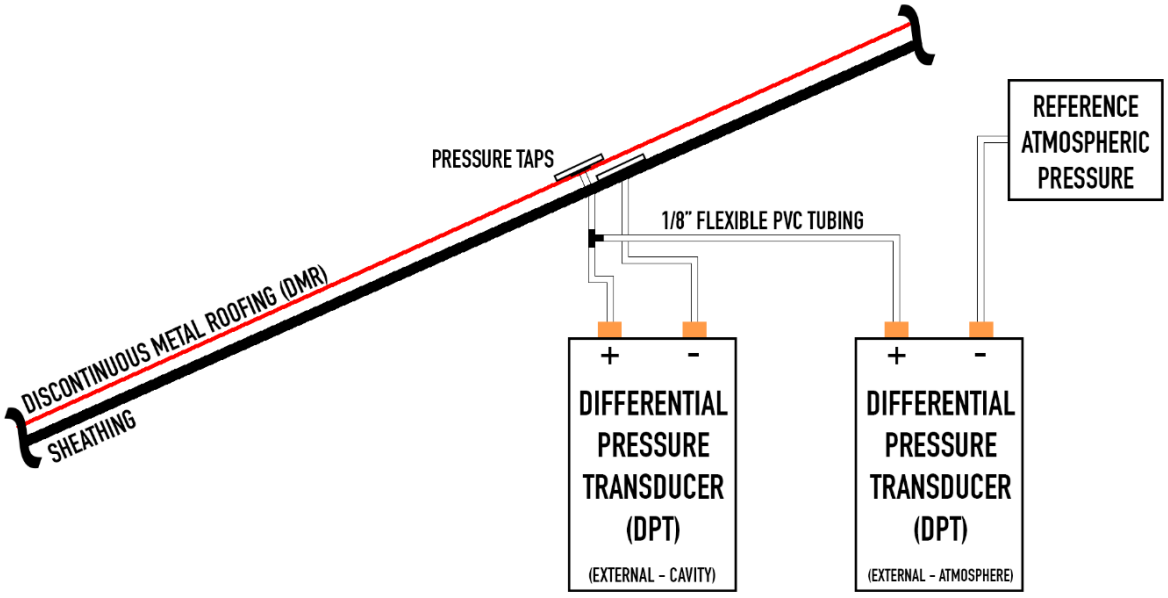

Figure 4. *Schematic of the pressure tap locations and pressure transducer configuration to measure both net and external pressures simultaneously.*

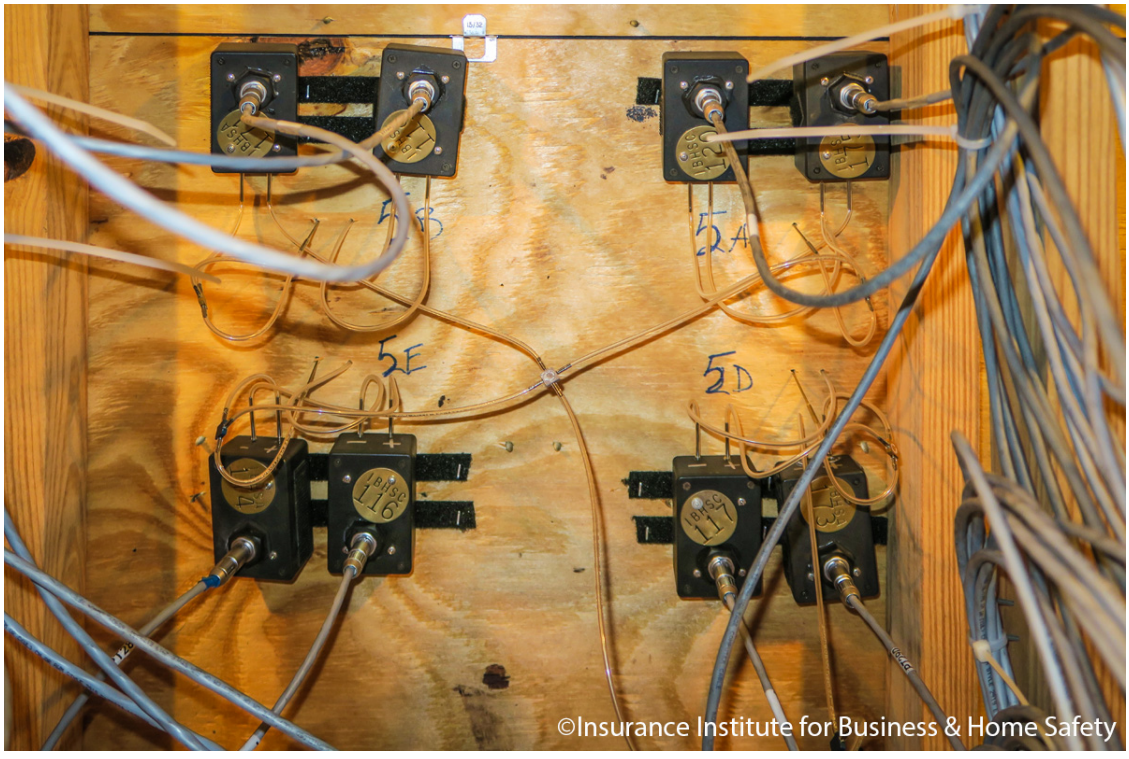

Figure 5. *Pressure transducers installed inside the building for four pressure tap locations on a single panel.*

Test Plan

The purpose of this study was to simply examine the wind forces acting on the two DMR without consideration of specific product performance or ultimate capacities (i.e., failures). Therefore, all tests presented herein were conducted at a mean roof height wind speed of 50 mph. The building was tested over a full 360 degrees at 10-degree increments so that each DMR product was tested to identical, relative wind angles. Figure 3 provides the wind angle convention (θ) used in this study. At each wind angle, wind pressure data was collected at a sampling rate of 100 Hz for a duration of 900 seconds.

Data Reduction

The pressure time histories obtained for each pressure transducer was converted into GCp_{eq} values that are comparable to *GCp* values provided by ASCE 7-10 (2010). The results presented as GCp_{eq}^{ext} refer to the measured external pressures, while GCp_{eq}^{net} refers to the net pressure across the panels. While comparisons can be made between the measured GCp_{eq}^{ext} and the *GCp* values provided in ASCE 7-10 (2010), the focus of this study was to examine the net and pressure equalization factors of the roofing products. As such, the placement of the instrumentation is not optimized for a full and rigorous comparison to the design *GCp* values provided in ASCE 7-10 (2010). This study presents statistical peak coefficients rather than the absolute highest coefficient. This methodology is often used when reporting peak pressures from wind tunnel results. Refer to Gavanski et al. (2016) for a more detailed discussion. To obtain these statistical peaks, the pressure time histories are divided into five segments. The peaks from each segment are extracted and fit with a Gumbel distribution using the Lieblein BLUE (best linear unbiased estimators) method (1974). The peak values reported herein are 78th percentile values from the Gumbel distribution. Unless otherwise indicated, the PEF values reported are then calculated using these statistical peak external and net pressures.

Results

Statistical peaks for each pressure time history were determined using the method described in the previous section. For typical cladding elements on the roof, the suction pressures are the most critical for design. As such, the peak pressures discussed below refer to the peak suction (negative) pressures experienced by the products.

Figure 6 presents mean and peak GCp_{eq}^{ext} and GCp_{eq}^{net} for Panel 29 (DMR1) vs. wind angle. The peak coefficient from each segment of the pressure time history used for the statistical fitting is also shown in Figure 6. Similarly, Figure 7 shows the same results for Panel 1 (DMR2). Figures 6 and 7 show similar trends between GCp_{eq}^{ext} and GCp_{eq}^{net}; however, the ratio between the net and external pressure varies based on wind angle. Figure 8 shows a summary of PEF vs. GCp_{eq}^{ext} , using the fitted peaks over all wind angles and panels for DMR1. A PEF of 0.7 appears to envelope the PEF values at higher external pressures and is shown as a black horizontal line in Figure 8. Similarly, Figure 9 presents the PEF vs. GCp_{eq}^{ext} for DMR2, where a PEF of 0.7 also appears to envelope the PEF at higher external pressures. The similarity in PEF values between the two DMR systems is surprising given the differences between the two products and the geometry of the cavity space beneath the panels. The similarity suggests that the PEFs for DMR products may be more similar than for wall cladding products observed by Morrison and Cope (2015); however, more research would be needed to validate this hypothesis.

Tables 1 and 2 provide a summary of the fitted peaks GCp_{eq}^{ext} and GCp_{eq}^{net} along with PEF for the worst wind angles for all panels shown in Figures 8 and 9. It should be noted that certain panels shown in Figure 3 were omitted from this analysis due to bad data from one or more pressure taps on the panel. Also, all peak, net and external pressures presented so far have been the peak and net pressures at the instant in time when the external pressure is largest (negative). However, since the peak external and peak net pressures may not necessarily occur at the same instant in time, the last column in Table 1 and Table 2 also presents a PEF based on the absolute GCp_{eq}^{net} and GCp_{eq}^{ext} even if they do not occur at the same time. For certain panels, using the absolute highest GCp_{eq}^{net} and GCp_{eq}^{ext} to calculate the PEF is conservative; however, for those panels that have the largest PEF, i.e., where the DMR sees the highest percentage of the external pressure, there is no difference in results obtained using the two approaches.

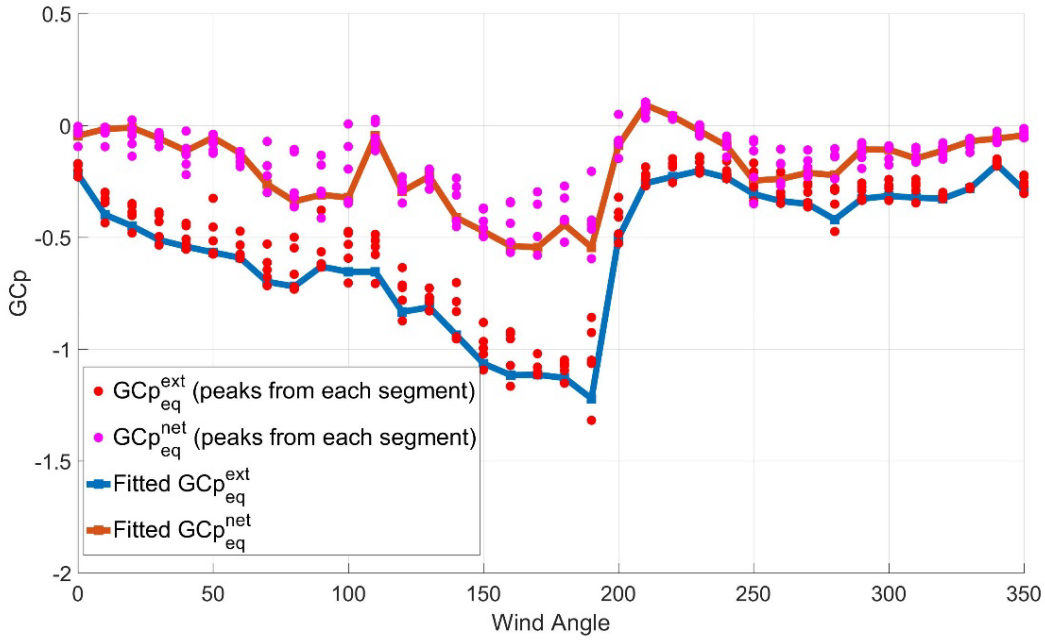

Figure 6. *Fitted peak* $\boldsymbol{GCp_{eq}^{net}}$ *and* $\boldsymbol{GCp_{eq}^{ext}}$ *with the corresponding peak values from each segment of the pressure time history vs. wind angle for Panel 29 (DMR1).*

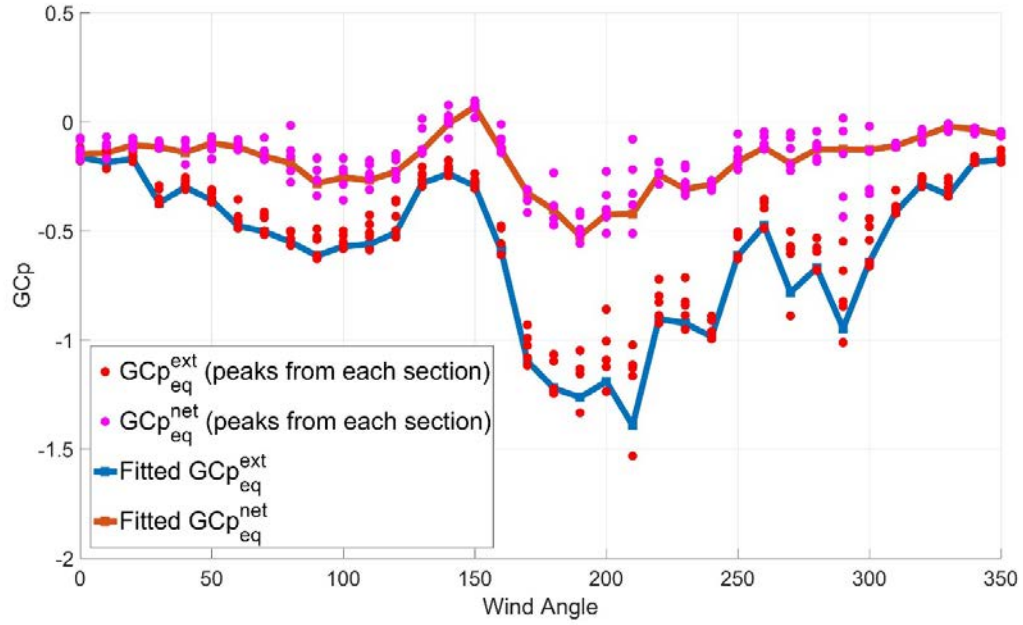

Figure 7. *Fitted peak* $\boldsymbol{GCp_{eq}^{net}}$ *and* $\boldsymbol{GCp_{eq}^{ext}}$ *with the corresponding peak values from each segment of the pressure time history vs. wind angle for Panel 1 (DMR2).*

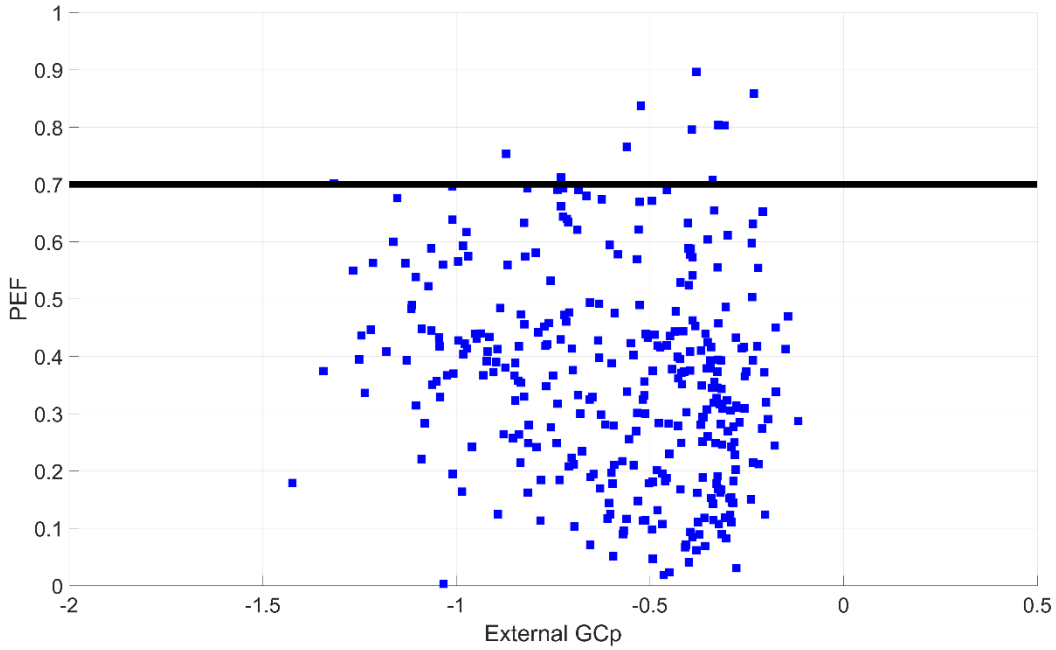

Figure 8. *PEF vs.* $\boldsymbol{GCp_{eq}^{ext}}$ *for all DMR1 panels and all wind angles tested.*

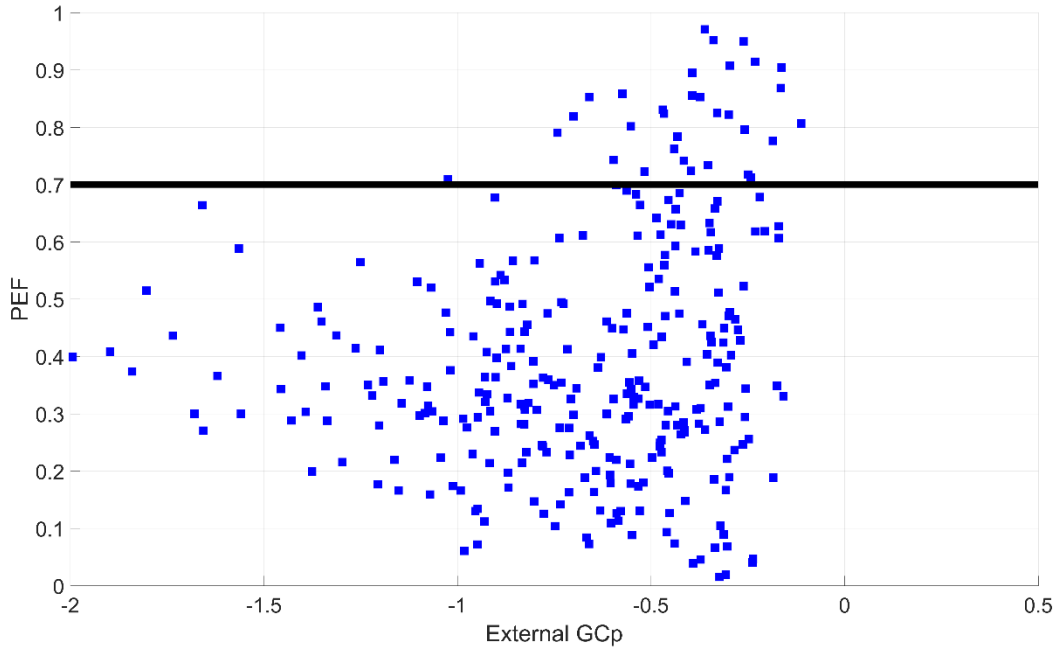

Figure 9. *PEF vs.* $\boldsymbol{GCp_{eq}^{ext}}$ *for all DMR2 panels and all wind angles tested.*

Table 1. Summary of largest GCp_{eq}^{net}, GCp_{eq}^{ext} and PEF for DMR1

Panel	Fitted GCp_{eq}^{ext}	**Corresponding** GCp_{eq}^{net}	GCp_{eq}^{net} **/ Highest** GCp_{eq}^{ext} **(PEF)**	**Highest** GCp_{eq}^{net} **/ Highest** GCp_{eq}^{ext} **(PEF)**
29	-1.318	-0.596	0.452	0.473
31	-0.876	-0.297	0.339	0.595
36	-1.427	-1.031	0.722	0.722
38	-1.183	-0.667	0.564	0.652
42	-1.233	-0.760	0.616	0.616
52	-0.998	-0.406	0.407	0.581
54	-0.887	-0.516	0.581	0.634
58	-1.491	-0.253	0.170	0.427
60	-1.463	-0.577	0.394	0.487
61	-1.321	-0.608	0.460	0.464

Table 2. Summary of largest GCp_{eq}^{net}, GCp_{eq}^{ext} and PEF for DMR2

Panel	Fitted GCp_{eq}^{ext}	**Corresponding** GCp_{eq}^{net}	GCp_{eq}^{net} **/ Highest** GCp_{eq}^{ext} **(PEF)**	**Highest** GCp_{eq}^{net} **/ Highest** GCp_{eq}^{ext} **(PEF)**
1	-1.532	-0.513	0.335	0.365
2	-0.960	-0.363	0.378	0.503
7	-1.057	-0.172	0.163	0.596
8	-2.001	-0.833	0.414	0.494
11	-0.961	-0.569	0.592	0.665
13	-1.798	-1.246	0.693	0.693
15	-2.037	-0.773	0.379	0.515
22	-1.772	-0.459	0.259	0.414
25	-1.203	-0.215	0.179	0.549

Conclusion

Both net and external wind pressures were measured on two DMR systems installed on a full-scale, steep-slope building and tested in IBHS' large test chamber. The results from this study show that the highest loaded panels for both systems experienced about 70% of the total external pressure. Despite the similarity in PEF for the two systems tested, other DMR systems with different sizes, assembly methods, air pathways and cavity geometries may have different results. The recent work by Miller at al. (2017) has shown that PEF can be determined using an airbox technique, provided that the benchmark full-scale data like that obtained in this study is available.

References

American Society for Civil Engineers. (2010). *ASCE 7-10: Minimum Design Loads for Buildings and Other Structures.* Reston, VA: American Society of Civil Engineers.

ASTM D3679. (2013). *Standard Specification for Rigid Poly (Vinyl Chloride) (PVC) Siding*. West Conshohocken, PA: ASTM International.

Gavanski, E., Gurley, K.R., and Kopp, G.A. (2016). Uncertainties in the Estimation of Local Peak Pressures on Low-Rise Buildings by Using the Gumbel Distribution Fitting Approach. *Journal of Structural Engineering,* 142(11). doi:10.1061/(ASCE)ST.1943-541X.0001556

Lieblein, J. (1974). "Efficient methods of extreme-value methodology." NBSIR 74-602, National Bureau of Standards, Washington, DC.

Miller, C.S., Kopp, G.A., Morrison, M.J., Kemp, G., and Drought, N. (2017). A Multichamber, Pressure-Based Test Method to Determine Wind Loads on Air-Permeable, Multilayer Cladding Systems. *Frontiers in the Built Environment,* 3:7. doi:10.3389/fbuil.2017.00007

Morrison M.J., and Cope A.D. (2015). "Wind Performance and Evaluation Methods of

Multi-Layered Wall Assemblies," *Proceeding of ASCE Structures Congress.* Portland, OR, pp. 2735-2748.

Oh, J.H., and Kopp, G.A. (2014). Modelling of spatially and temporally-varying cavity pressures in air permeable, double-layer roof systems. *Building and Environment,* 82, 135-150. doi:10.1016/j.buildenv.2014.08.008

Standohar-Alfano, C. D., Estes, H., Johnston, T., Morrison, M. J., and Brown-Giammanco, T. M. (2017). Reducing Losses from Wind-Related Natural Perils: Research at the IBHS Research Center. *Frontiers in the Built Environment,* 3:9. doi:10.3389/fbuil.2017.00009

Appendix A

Table 3. Panel numbers and number of pressure tap locations for each product

DMR1		DMR2	
Panel Number	Number of Tap Locations	Panel Number	Number of Tap Locations
28	1	1	6
29	6	2	6
30	1	3	1
31	6	4	1
32	1	5	6
33	1	6	1
34	1	7	6
35	1	8	6
36	6	10	6
37	1	11	6
38	6	12	1
39	1	13	6
40	1	14	6
41	1	15	6
42	6	16	1
43	1	17	6
44	1	18	1
45	1	19	6
46	6	20	1
47	1	21	6
48	1	22	6
49	1	23	1
50	1	24	1
51	1	25	6
52	6	26	1
53	1	27	6
54	6		
55	1		
56	1		
57	1		
58	6		
59	1		
60	6		
61	6		
62	1		
63	1		